Inorg. Chem. **2008**, *47*, 8839−8846

Nature of Catalytic Activities of CoO Nanocrystals in Thermal Decomposition of Ammonium Perchlorate

Liping Li, Xuefei Sun, Xiaoqing Qiu, Jiaoxing Xu, and Guangshe Li*

State Key Laboratory of Structural Chemistry, Fujian Institute of Research on the Structure of Matter, Chinese Academy of Sciences, Fuzhou 350002, P.R. China

Received May 7, 2008

This work addresses the chemical nature of the catalytic activity of X-ray "pure" CoO nanocrystals. All samples were prepared by a solvothermal reaction route. X-ray diffraction indicates the formation of CoO in a cubic rock-salt structure, while infrared spectra and magnetic measurements demonstrate the coexistence of CoO and Co_3O_4. Therefore, X-ray "pure" CoO nanocrystals are a unique composite structure with a CoO core surrounded by an extremely thin Co_3O_4 surface layer, which is likely a consequence of the surface passivation of CoO nanocrystals from the air oxidation at room temperature. The CoO core shows a particle size of 22 or 280 nm, depending on the types of the precursors used. This composite nanostructure was initiated as a catalytic additive to promote the thermal decomposition of ammonium perchlorate (AP). Our preliminary investigations indicate that the maximum decomposition temperature of AP is significantly reduced in the presence of CoO/Co_3O_4 composite nanocrystals and that the maximum decomposition peak shifts toward lower temperatures as the loading amount of the composite nanocrystals increases. These findings are different from the literature reports when using many nanoscale oxide additives. Finally, the decomposition heat for the low-temperature decomposition stages of AP was calculated and correlated to the chemical nature of the CoO/Co_3O_4 composite nanostructures.

1. Introduction

CoO and Co_3O_4 are two typical crystalline forms of the Co−O system[1−4] that show many interesting electronic and magnetic properties for a wide variety of scientific and technological applications.[5−7] Various methodologies[1−3,8−12] including sol−gel, microemulsion, thermal decomposition in inert gas, and hydrogen reduction have been developed for the preparation of cobalt oxides. Navrotsky et al.,[11] prepared CoO nanocrystals by thermal decomposition of cobalt hydroxide in a H_2/Ar atmosphere, while it is not clear if surface oxidation is entirely avoided. Wang et al.,[13] prepared a mixture of nanocrystals that contains Co, Co_3O_4, and CoO at 130 °C using Na(AOT) as the surfactant. By heating an aqueous solution of $Co(OH)_2$ at 273 °C under vacuum, Co_3O_4 is still observable in the final products.[14] As a result, Co_3O_4 seems indispensable for the formation of CoO nanocrystals,[15] which may produce uncertain contributions to the properties of CoO nanocrystals.

To avoid surface oxidation, many kinds of surfactants[16−19] have been studied. Nevertheless, most of these methods are complicated, and the frequent use of surfactants has led to the deteriorated chemical and physical properties. Generally,

* To whom correspondence should be addressed. E-mail: guangshe@fjirsm.ac.cn. Phone: +86-591-83792846. Fax: +86-591-83702122.

(1) Chidambaram, K.; Malhotra, L. K.; Chopra, K. L. *Thin Solid Films* **1982**, *87*, 365.
(2) Eze, F. C. *J. Phys. D: Appl. Phys.* **1999**, *32*, 533.
(3) Patil, P. S.; Kadam, L. D.; Lokhande, C. D. *Thin Solid Films* **1996**, *272*, 29.
(4) Brundle, C. R.; Chuang, T. J.; Rice, D. W. *Surf. Sci.* **1976**, *60*, 286.
(5) Hagelin-Weaver, H. A. E.; Hoflund, G. B.; Minahan, D. M.; Salaita, G. N. *Appl. Surf. Sci.* **2004**, *235*, 420.
(6) (a) Patil, P. S.; Kadam, L. D.; Lokhande, C. D. *Sol. Energy Mater. Sol. Cells* **1998**, *53*, 229. (b) Gallant, D.; Pezolet, M.; Simard, S. *J. Phys. Chem.B* **2006**, *110*, 6871.
(7) Barreca, D.; Massignan, C.; Daolio, S.; Fabrizio, M.; Piccirillo, C.; Armelao, L.; Tondello, E. *Chem. Mater.* **2001**, *13*, 588.
(8) Zhang, L. Y.; Xue, D. S. *Chin. J. Rare Met.* **2003**, *27*, 547.
(9) Guan, J. Y.; Zhao, Y.; Hou, S. F. *J. Hebei Normal University* **1999**, *23*, 90.
(10) Do, J. S.; Weng, C. H. *J. Power Sources* **2005**, *146*, 482.
(11) Wang, L.; Vu, K.; Navrotsky, A.; Stevens, R.; Woodfield, B. F.; Boerio-Goates, J. *Chem. Mater.* **2004**, *16*, 5394.
(12) Gulino, A.; Dapporto, P.; Rossi, P.; Fragala, I. *Chem. Mater.* **2003**, *15*, 3748.
(13) Yin, J. S.; Wang, Z. L. *Phys. Rev. Lett.* **1997**, *29*, 570.
(14) Gravelle, P. C.; Teichner, S. *Adv. Catal.* **1969**, *20*, 167.
(15) Lawecka, M.; lawska-Waniewska, A.; Racka, K.; Leonowicz, M.; Dzhardimalieva, I.; Rozenberg, A. S.; Pomogailo, A. D. *J. Alloys Compd.* **2004**, *369*, 244.

10.1021/ic8008283 CCC: $40.75
Published on Web 09/03/2008

the chemical and physical properties of the solids are governed by particle size, phase composition, and surface chemical states. For instance, with regards to the particle size effects, bulk CoO crystallizes in a cubic structure and is antiferromagnetic with a Neel temperature of $T_N = 298$ K. When the particle size of CoO reduces to the nanoscale regime, the core will be antiferromagnetically ordered, while the surface spins become significant to dominate the magnetic behavior. Moreover, the magnetic transition temperature T_N is reduced to 25 K for 1.5 nm CoO film.[20] Recently, CoO nanocrystals were taken as the positive electrode, which have shown excellent specific capacity and discharge voltage.[21] Even so, the knowledge about the chemical nature of CoO nanocrystal is very limited comparing with the metallic Co, Co_3O_4, or other complex cobalt oxides.

We anticipate that the chemical nature of CoO nanocrystals could be preliminarily understood by examining the catalytic roles of CoO nanocrystals in the thermal decomposition of AP. This is because (1) AP is one of the main oxidizing agents that have been used in various propellants and the burning behaviors of propellants are highly relevant to the thermal decomposition of AP and because (2) extensive literature work has shown that nanoscale metals (like Co) can significantly improve the AP decomposition.[22,23] These nanoscale metals will be oxidized into the corresponding metal oxides such as CoO by the oxidizing gases like O_2, NO, and N_2O that are released during AP decomposition.[23] (3) The metal oxides like CoO and Co_3O_4 exhibit high and stable catalytic activity and selectivity toward the oxidation of ammonia,[24] the intermediate product of AP decomposition, and thus are promising in promoting the sufficient AP decomposition. With this in mind, we expect that CoO nanocrystals coated with Co_3O_4 layers may exhibit excellent catalytic activity toward AP decomposition. As a consequence, the nature associated with the catalytic actvity of CoO nanocrystals becomes the motive of this work.

In this work, we used a simple solvothermal method to prepare CoO nanocrystals that were coated by thin Co_3O_4 layers. By XRD and magnetic susceptibility measurements, the phase features of products were determined and discussed. The catalytic roles of CoO−Co_3O_4 composite nanostructure toward AP decomposition were also explored.

2. Experimental Section

Cobalt acetate tetrahydrate ($Co(CH_3COO)_2 \cdot 4H_2O$), sodium hydroxide (NaOH), hydrazine hydrate ($N_2H_4 \cdot H_2O$), and absolute ethanol (C_2H_5OH) were used as the starting materials for all sample syntheses. CoO nanocrystals were prepared using the following methods.

Method I. A 50 mL NaOH solution with a concentration of 5 mol/L was dropped into a mixed pink solution of 0.01 mol $Co(CH_3COO)_2 \cdot 4H_2O$ with 100 mL distilled water under continuous stirring. After the mixture was stirred for 10 min, a brown suspension appeared, which was then filtered and sufficiently washed with distilled water to remove the CH_3COO^- and Na^+ ions that may contaminate the sample surfaces. After sufficient washing, the precipitate was redispersed into 150 mL ethanol using supersonication to get a uniform suspension, which was transferred to Teflon-lined stainless steel autoclaves with a capacity of 30 mL and reacted at a selected temperature in the range of 180−220 °C for 24 h. After the reaction mixture was cooled to room temperature, a black solid was collected by filtration, washed with distilled water for several times, and dried in air at ambient condition. The samples prepared at 200 °C were named as sample I.

Method II. Three milliliters of hydrazine was added dropwise into a mixed pink solution of 0.01 mol $Co(CH_3COO)_2 \cdot 4H_2O$ with 100 mL distilled water under continuous stirring. This solution was completely transferred into autoclaves to react at 200 °C for 2 h. After washing and drying according to the proceedures for sample I, we obtained sample II.

Phase compositions of the samples were characterized by powder X-ray diffraction (XRD) at room temperature on a Rigaku D/MAX25000 diffractometer with a copper target. The morphologies of the samples were investigated by transmission electron microscopy (TEM) on a JEM-2010 apparatus with an acceleration voltage of 200 kV. The infrared spectra of the samples were measured with a Perkin-Elmer IR spectrophotometer (Spectrum One) at a resolution of 4 cm^{-1} using the KBr pellet technique. Thermal behaviors of the samples were examined using STA449C coupled with Jupiter-QMS 403C Aeolos in nitrogen atmosphere at a heating rate of 15 °C/min. The magnetic properties of the samples were measured using a Quantum Design PPMS-7 magnetometer.

The catalytic roles of CoO nanocrystals in the thermal decomposition of AP were studied by differential scanning calorimeter (DSC) using DTA404PC in N_2 atmosphere over the temperature range of 30−500 °C. To investigate the influence of dosage of CoO nanocrystals on AP decomposition, AP and CoO nanocrystals were premixed at a mass ratio ranging from 99:1 to 90:10 to prepare the target samples. The activation energies of AP decomposition with and without additives of CoO nanocrystals were measured by varying the heating rates. A total sample mass of 3.0 mg was used for all runs.

3. Results and Discussion

Figure 1 shows XRD patterns of the samples prepared using Methods I and II. It is seen that all diffraction peaks are in good agreement with the standard diffraction data for CoO, while no diffractions from the impurities Co_2O_3 or Co_3O_4 were observed. These results indicated that the products prepared by these methods are X-ray pure CoO in a cubic rock-salt structure. It is noted that when using Method

(16) An, K.; Lee, N.; Park, J.; Kim, S. C.; Hwang, Y.; Park, J.-G.; Kim, J.-Y.; Park, J.-H.; Han, M. J.; Yu, J.; Hyeon, T. *J. Am. Chem. Soc.* **2006**, *128*, 9753.

(17) Seo, W. S.; Shim, J. H.; Oh, S. J.; Lee, E. K.; Hur, N. H.; Park, J. T. *J. Am. Chem. Soc.* **2005**, *127*, 6188.

(18) Zhan, Y. J.; Yin, C. R.; Wang, W. Z.; Wang, G. H. *Mater. Lett.* **2003**, *57*, 3402.

(19) (a) Glaspell, G. P.; Jagodzinski, P. W.; Manivannan, A. *J. Phys. Chem. B* **2004**, *108*, 9604. (b) Soriano, L.; Abbate, M.; Ferna′ndez, A.; Gonza′lez-Elipe, A. R.; Sirotti, F.; Sanz, J. M. *J. Phys. Chem. B* **1999**, *103*, 6676.

(20) Ivanov, B. A.; Kolezhuk, A. K.; Wysin, G. M. *Phys. Rev. Lett.* **1996**, *76*, 511.

(21) Wu, J. B.; Tu, J. P.; Tu, J. P.; Wang, X. L.; Zhang, W. K. *Int. J. Hydrogen Energy* **2007**, *32*, 606.

(22) Liu, L. L.; Li, F. S.; Tan, L. H.; Ming, L.; Yi, Y. *Propellants, Explos., Pyrotech.* **2004**, *29*, 34.

(23) Duan, H. Z.; Lin, X. Y.; Liu, G. P.; Xu, L.; Li, F. S. *Chin. J. Chem. Eng.* **2008**, *16*, 325.

(24) (a) Matatov-Meytal, Y.; Sheintuch, M. *Ind. Eng. Chem. Res.* **1998**, *37*, 309. (b) Schmidt-Szalowski, K.; Krawczyk, K.; Petryk, J. *Appl. Catal., A* **1998**, *175*, 147.

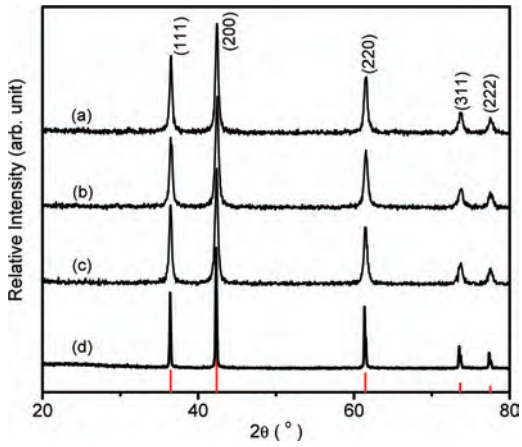

Figure 1. XRD patterns of the samples prepared using Method I at temperatures of (a) 180, (b) 200 °C, and (c) 220 °C or using Method II at (d) 200 °C. Red vertical bars represent the standard diffraction data for cubic CoO from JCPDS file (No. 43-1004).

I, the half-height widths of the diffraction peaks (200) were almost the same (Figure 1a−c) when the reaction temperature varied in the temperature range from 180 to 220 °C. The crystallite sizes for the samples were calculated to be about 22 nm using Scherrer formula for the main peak (200), which is confirmed by TEM observations. It is obvious that reaction temperature has little influence on the crystallite size of CoO nanocrystals when using Method I. As indicated by TEM observations, Sample I exhibited a thin nanosheet morphology with a particle size of about 25 nm (Figure 2a), which is apparently different from the hexagonal and cubic CoO nanocrystals reported by Seo et al.[17] using a single precursor $Co(acac)_3$ (acac = acetylacetonate). These nanosheets are small single crystals with high crystallinity as indicated by the corresponding high resolution TEM photos (Figure 2b). Here, it is very difficult to distinguish thin Co_3O_4 layers if any, from CoO because of the much smaller particle size. Interestingly, for sample II, 280 nm CoO thus obtained is also composed of tiny single crystals with the dimension approximately ten times larger than that of sample I (Figure 2c). The interplanar spacing of the tiny single crystals was about 0.247 nm (Figure 2d), which corresponds to that for two adjacent (111) planes of cubic CoO. Further, 2-D lattice fringes at the edge of single crystals demonstrate the presence of a thin film of Co_3O_4 on surfaces of CoO nanocrystals.

What is the reason for such a big difference in the particle sizes for these preparation methods? Because the main difference in the preparation parameters of these samples is from the use of the base NaOH or hydrazine, it is necessary to investigate the roles that the basic species plays in the grain growth of the CoO nanocrystals. The formation reaction of CoO nanocrystals using Method I is thought to proceed in two steps as shown in eqs 1 and 2.

$$Co(CH_3COO)_2 + 2NaOH \rightarrow Co(OH)_2 + 2CH_3COONa \quad (1)$$

$$Co(OH)_2 \rightarrow CoO + H_2O \quad \text{at } 180-220\ ^\circ C \quad (2)$$

which are deduced from the intermediate products that appeared during the reaction states: In the first step, $Co(CH_3COO)_2$ solution mixed with NaOH and yielded a brown color precursor of β-$Co(OH)_2$, as is confirmed by XRD (Figure 3a). It is noted from Figure 3a that the diffraction peaks (h,k,l) with $h \neq 0$ including (100) and (110) are much narrower than those with $k = 0$; therefore the precursor β-$Co(OH)_2$ is highly oriented. The TEM observation confirms the sheet shape of the precursor β-$Co(OH)_2$ (Supporting Information). These sheet precursors decomposed under solvothermal conditions to yield sheet-like CoO nanocrystals. This inheriting morphology behavior is interesting, most likely because, for hexagonal structure β-$Co(OH)_2$, Co ions layers are separated by two adjacent layers of hydroxyl ions. Under solvothermal conditions, the hydrogen bonds associated with the two adjacent layers of hydroxyl ions might be partially broken to release certain amounts of water molecules. The oxygen ions left within these hydroxyl layers would rearrange their positions to one singular oxygen layer and produce the structural unit of CoO in a stacking sequence of ABCABC..., like that in the cubic rock-salt structure.[25] During this transformation, the framework constructed mainly by Co^{2+} ions was kept to show the inheriting morphology of the sheet shape. Therefore, the particle size of CoO was predominantly determined by the sheet precursor, while the impacts from the reaction temperature (180−220 °C) are relatively weaker. Comparatively, when using Method II, the formation mechanism of CoO nanocrystals is complicated because the $Co(CH_3COO)_2$ solution mixed with hydrazine yielded a pink suspension of an unknown complex (Figure 3b and Supporting Information). CoO nanocrystals were then formed after transformation of this complex under solvothermal reaction. These intermediates are likely responsible for the difference in particle sizes in the final CoO nanocrystals, although the reaction temperatures were kept the same.

The thermal behaviors of the samples were investigated by TG measurements under N_2 atmosphere. As indicated in Figure 4a, all samples showed a continuous mass loss below 600 °C, which amounts to about 7 wt % for sample I, almost double the amount of about 4 wt% for sample II. To determine what is responsible for the difference in mass loss, we did a mass spectroscopic (MS) analysis of the exhaust gases that accompanied with the mass loss during the heating process. As indicated in Figure 4b, with increasing the temperature, part of water molecules characterized by the MS signal at $m/z = 18$ was first released from the surfaces of CoO nanocrystals. When the temperature was varied in the range from 200 to 600 °C, the CO_2 signal at $m/z = 44$ was detected, in addition to the signals of $m/z = 18$ and 17 for water molecules, which indicates a simultaneous removal of chemisorbed water and decomposition of carbonate species. This conclusion is also confirmed by our IR spectral analysis (Figure 5). No signal at $m/z = 28$ was observed, indicating that no CO was formed during the heating of the as-prepared CoO nanocrystals. One primary reason for this important observation is that the as-prepared CoO is free of residual acetate species on surface surfaces. As a result, the

(25) Qiu, X. Q.; Li, G. S.; Li, L. P. *J. Mater. Res.* **2007**, *22*, 908.

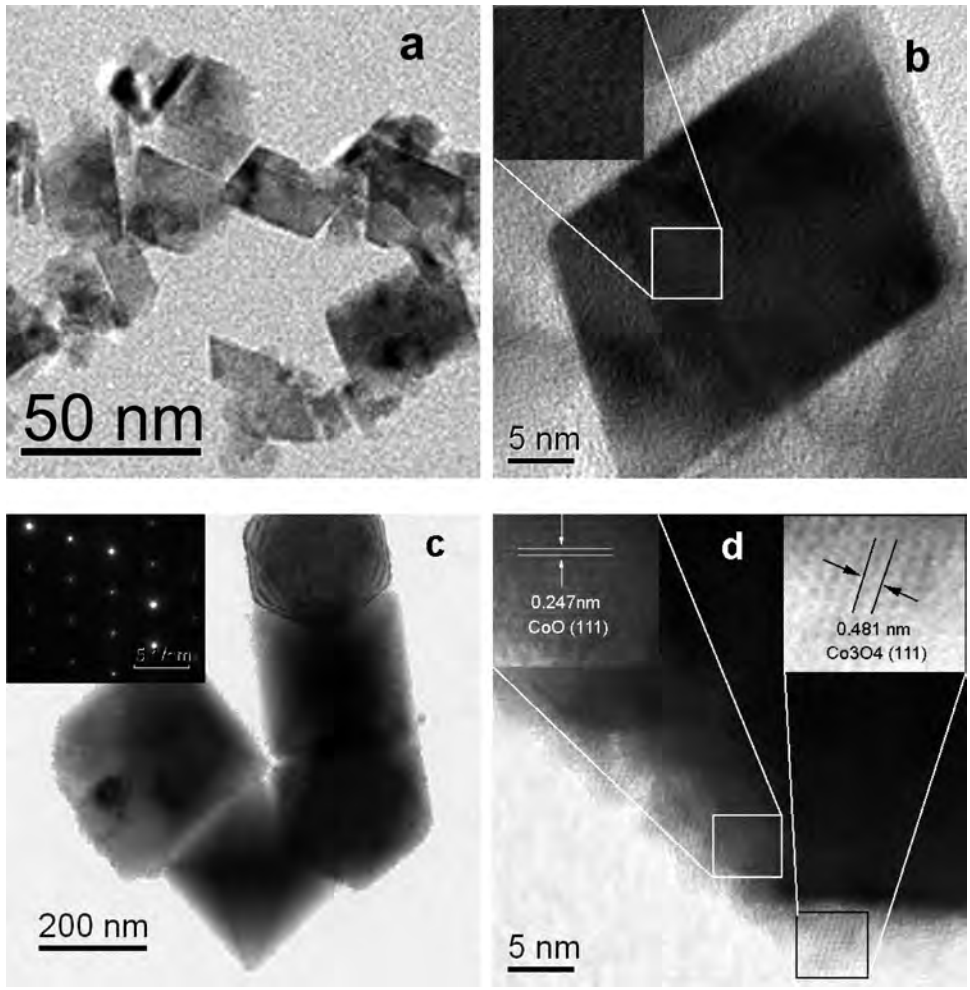

Figure 2. (a) TEM photos and (b) HRTEM image of samples I. (c) TEM photos and (d) HRTEM image of samples II. The insets of b and d are the enlarged HRTEM images. The inset of c is the selected-area electron diffraction pattern. The particle sizes of sample II are much larger than those of sample I.

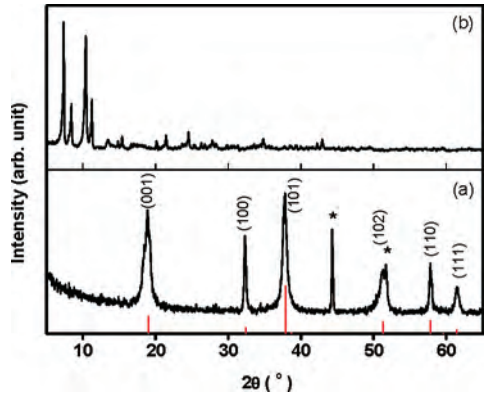

Figure 3. XRD patterns of the precursors that were produced when $Co(CH_3COO)_2$ solution mixed with (a) NaOH and (b) hydrazine. The diffraction peaks denoted by the asterisk (∗) are from internal standard Ni. Vertical bars represent the standard data of β-$Co(OH)_2$ (JCPDS, No. 30-0443).

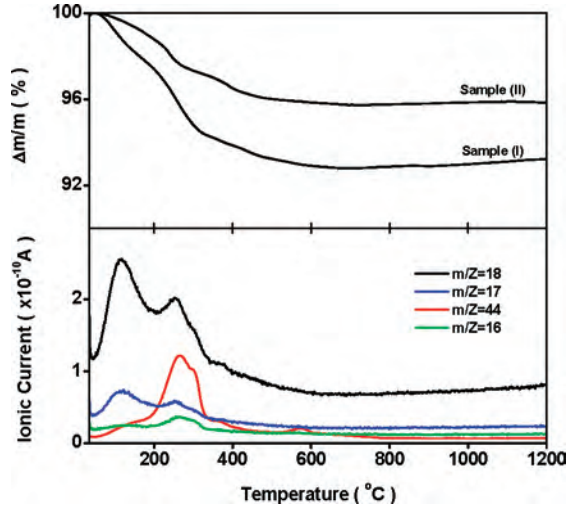

Figure 4. (a) TG curves of the samples I and II, as well as (b) mass spectra of the exhaust gases that were released during the heating process of sample I in N_2.

uncertainties in mass losses that may generate from CoO reduction to metallic Co can be completely excluded, because of the absence of the reducing gases, such as CO, or the active hydrogen that may be produced when CO reacts with the available water via the water-gas shift reaction. Consequently, the difference in mass loss should be associated with the activated sites for the absorbed water molecules and carbonates, which is apparently consistent with their particle sizes (or specific surface areas). It is interesting that above 600 °C, all samples showed almost constant mass, which differs from the CoO nanocrystals that were prepared by precipitation and thermal decomposition methods,[11] because

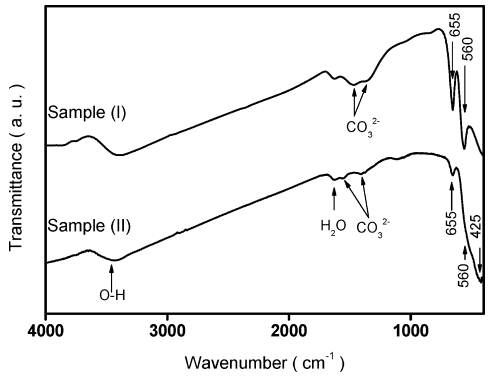

Figure 5. IR spectra of samples I and II.

for the later cases, an evident mass loss associated with the decomposition of the secondary phase Co_3O_4 was detected at 800 °C.[11] Obviously, the present solvothermal reaction can be an oxygen-poor condition, which gives rise to the majority phase of CoO nanocrystals.

It is well-known that CoO nanocrystals are kinetically unstable and would be readily oxidized to Co_3O_4. If traces of Co_3O_4 (<1 wt %) coexisted with the CoO nanocrystals, it could be very difficult to detect by XRD or TG technique because their detection limits are approximately 5 and 1 wt %, respectively. Here, we performed infrared spectra and magnetization analyses to determine whether the as-prepared CoO nanocrystals were terminated with other forms of cobalt oxides, such as Co_3O_4 or Co_2O_3. As indicated by the infrared spectra (Figure 5), all samples exhibited broad absorption bands at about 3440 and 1630 cm^{-1}, which correspond to the O−H stretching vibration and the bending mode of the absorbed water. A set of bands were observed in the range from 1570 to 1250 cm^{-1}, which are associated with the carbonate species. A band located at 425 cm^{-1} is assigned to the stretching vibration of Co−O bond in CoO with a rock-salt structure, while the two bands observed at 655 and 560 cm^{-1} are characteristic vibrations of Co^{2+}-O and Co^{3+}-O bond in Co_3O_4.[26] Both Sample (I) and Sample (II) gave a weaker absorption at 655 cm^{-1} and a shoulder at 560 cm^{-1}. Combined with our TG data analysis, it can be concluded that both physi- and chemisorbed water molecules are the principal surface species present in the as-prepared nanocrystals and that, in case of trace Co_3O_4, some carbonate species present on the surface of CoO nanocrystals as is reported in CoO_x-Al_2O_3 nanopowders.[27]

Figure 6 shows the temperature (T) dependence of the magnetization (M) and the magnetization versus magnetic field (H) behavior at 300 K of the as-prepared samples. For sample I, a maximum M was observed at low temperature of about 5 K. With increasing the temperature beyond 45 K, M slightly decreased, which does not follow the Curie−Weiss law. Therefore, a nonparamagnetic behavior is clearly indicated at low temperatures. The zero-field cooling (ZFC) and field cooling (FC) data (inset of Figure

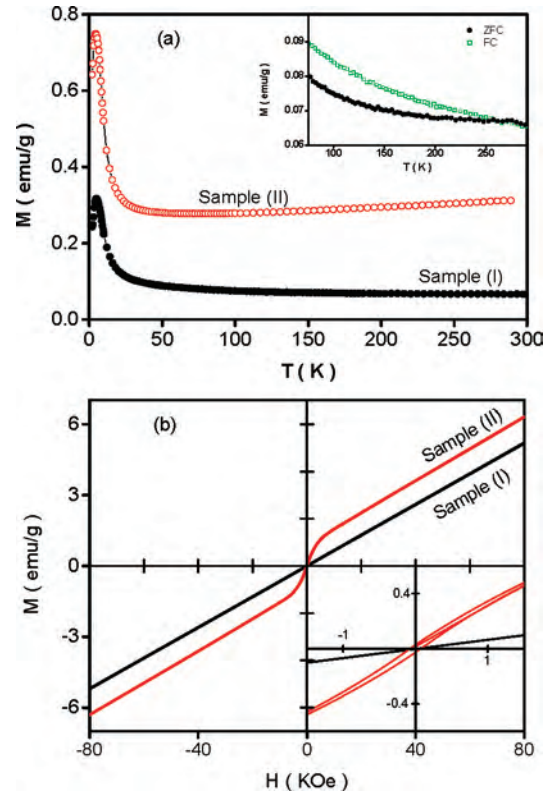

Figure 6. (a) Temperature dependence of zero-field cooled (ZFC) magnetization and (b) magnetization versus applied magnetic field at room temperature for samples I and II. Inset a shows the ZFC and FC magnetization versus temperature for sample I, and inset b shows the enlarged magnetization curves.

6a) became bifurcating at temperature of about 260 K, below which the magnetization in the FC process was enhanced over that in the ZFC process. It is noted that the bifurcating temperature is slightly lower than the Neel temperature of 290 K for bulk CoO but much higher than that of 40 K for bulk Co_3O_4.[28] At room temperature, no hysteresis loop was observed (Figure 6b), and M varied linearly with H, which demonstrates that sample I is paramagnetic at room temperature. These observations indicate a decrease of the ordering temperature and the possible presence of a superparamagnetic behavior below 260 K, consistent with the general observation that the ordering temperature for antiferromagnetic materials usually decreases as the particle size or dimension reduces.[29]

For sample II, a maximum M was also observed at about 5 K. Different from the slight decrease in M for sample I, the magnetization continuously increased as the temperature increased above 50 K, which is characteristic of antiferromagnetism as that for bulk CoO. The $M-H$ curves measured at room temperature demonstrate an obvious hysteresis loop with a coercivity of 76 Oe. No saturation magnetization was reached even under an external magnetic field of 8 T. These observations indicate the presence of ferromagnetic compo-

(26) Klepper, K. B.; Nilsen, O.; Fjellvag, H. *Thin Solid Films* **2007**, *515*, 7772.
(27) Azurdia, J.; Marchal, J.; Laine, R. M. *J. Am. Ceram. Soc.* **2006**, *89*, 2749.
(28) Gangopadhyay, S.; Hadjipanayis, G. C.; Sorensen, C. M.; Klabunde, K. J. *J. Appl. Phys.* **1993**, *73*, 6964.
(29) Zheng, X. G.; Xu, C. N.; Nishikubo, K.; Nishiyama, K.; Higemoto, W.; Moon, W. J.; Tanaka, E.; Otabe, E. S. *Phys. Rev. B* **2005**, *72*, 014464.

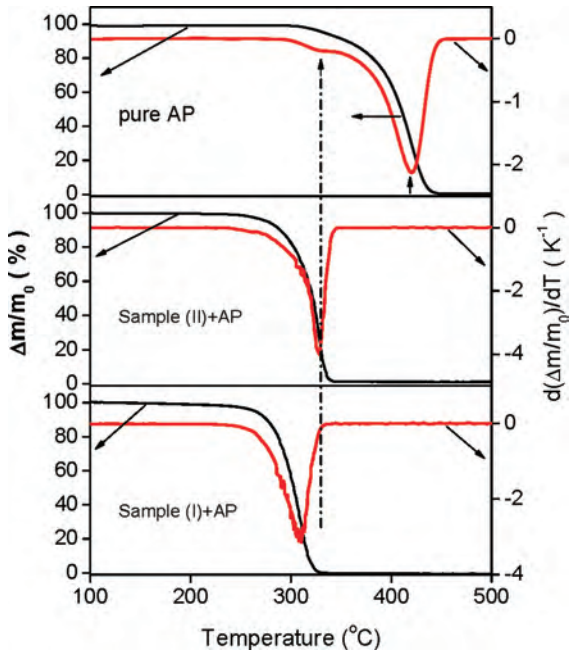

Figure 7. TG curves measured using aluminum pans without lids for pure AP and mixtures of AP with 2 wt % CoO nanocrystals that were prepared using different methods. Red lines are the first derivative curves of the raw TG data.

nent superimposed with a paramagnetic one. When these observations are compared with the observations for sample I, it can be deduced that the paramagnetic component is primarily originated from CoO with a small particle size. With regard to the common feature of a maximum *M* observed at about 5 K for both samples, it has to be stressed that similar behavior has also been reported for CoO nanorods.[16] But still, this maximum cannot be intrinsic for CoO phase, because (1) bulk CoO is an antiferromagnetic semiconductor with an ordering temperature of 290 K. Particle size reduction can only decrease the ordering temperature, as is observed for other antiferromagnetic materials such as CuO and NiO.[29] (2) In addition to CoO nanorods,[16] 20 nm Co_3O_4 was also reported to show a sharp peak in the ZFC data near 25 K,[30] and (3) similar peak structures have been observed in the magnetization data of MnO nanocrystals caused by the existence of a small amount of Mn_3O_4.[31] Therefore, it is most likely that traces of Co_3O_4 exist on the surface of CoO nanocrystals.

The as-prepared CoO nanocrystals were initially studied as an additive in promotion of the thermal decomposition of AP with an attempt to understand the chemical nature of the CoO nanocrystals. Figure 7 shows the raw TG data and their first derivative curves for AP with and without involving the as-prepared CoO nanocrystals. For pure AP, the thermal decomposition proceeded in two steps as clearly indicated in its first derivative curve. The first step started at about 290 °C and showed a peak at 328 °C in derivative curve of raw TG data, which is named as the low-temperature decomposition (LTD). The second step started at about 350 °C, showing a peak at 420 °C in the first derivative curve, which is assigned to the high-temperature decomposition (HTD). It is well established[32,33] that LTD involves a heterogeneous process which includes proton transfer in the AP subsurface to yield NH_3 and $HClO_4$, the capture of $HClO_4$ by proton trap ClO_3^- in the defect-bearing site of the lattice, and the decomposition of $HClO_4$. Alternatively, HTD is associated with the simultaneous dissociation and sublimation of AP to $HClO_{4(g)}$ and $NH_{4(g)}$.[34] For the present work, it is surprising that, when AP was mixed with our as-prepared CoO nanocrystals, the HTD process disappeared completely. In the case of the additives of sample II, the sole LTD process showed a peak temperature much closer to that observed for pure AP, which was however significantly reduced when involving additives of sample I. As a consequence, CoO nanocrystals could be used as an additive to accelerate the AP decomposition. Similar effects have been found for metallic Co nanocrystals and other transition metal nanooxides like CuO, NiO, and MnO.[35,23]

Heat released during AP decomposition with and without involving CoO nanocrystal additives is measured by DSC in a flowing atmosphere of nitrogen gas. Figure 8 shows the DSC curves of the mixture of AP with different amounts of sample I. DSC curves of pure AP are also given in Supporting Information for comparison. For pure AP, three DSC peaks were observed with or without lids. The first endothermic peak appeared at about 245 °C, which is associated with a phase transition of AP from orthorhombic to cubic because no mass changes appeared in the corresponding temperature range. The second peak is exothermic, which exactly corresponds to the LTD process. The third peak is referred as HTD process, which can be either exothermic or endothermic, depending on the use of lids.[34]

Such cases were apparently altered when as-prepared CoO nanocrystals or pure Co_3O_4 nanocrystals were added to AP. As shown in Figure 8 and Supporting Information, with the addition of the cobalt oxide nanocrystals, HTD process of AP disappeared to show a sole exothermic process in the temperature range from 260−380 °C with or without lids, though no change was observed for the phase transition temperature of AP. From the integral area of the exothermic process, the decomposition heat of AP is determined. In the presence of the additives of 18 nm Co_3O_4, AP showed a decomposition heat of 937 J/g and a maximum decomposition temperature of 325 °C with lids. Strikingly, in the case of CoO nanocrystals terminated with very thin layers of Co_3O_4 (sample I), the decomposition heat of AP increased up to 1427 J/g, which is accompanied by a apparent decrease of the maximum decomposition temperature to 308 °C. AP decomposition is also highly dependent on the amounts of CoO nanocrystals loaded and the use of the lids. With

(30) Makhlouf, S. A. *J. Magn. Magn. Mater.* **2002**, *246*, 184.
(31) Park, J.; Kang, E.; Bae, C. J.; Park, J. G.; Noh, H. J.; Kim, J. Y.; Park, J. H.; Park, H. M.; Hyeon, T. *J. Phys. Chem. B* **2004**, *108*, 13594.
(32) Boldyrev, V. V. *Thermochim. Acta* **2006**, *443*, 1.
(33) Reid, D. L.; Russo, A. E.; Carro, R. V.; Stephens, M. A.; LePage, A. R.; Spalding, T. C.; Petersen, E. L.; Seal, S. *Nano Lett.* **2007**, *7*, 2157.
(34) Vyazovkin, S.; Wight, C. A. *Chem. Mater.* **1999**, *11*, 3386.
(35) (a) Ma, Z. Y.; Li, F. S.; Chen, A. S.; Bai, H. P. *Acta Chem. Sin.* **2004**, *62*, 1252. (b) Chen, L. J.; Li, G. S.; Li, L. P. *J. Therm. Anal. Calorim.* **2008**, *2*, 581. (c) Duan, G. R.; Yang, X. J.; Chen, J.; Huang, G. H.; Lu, L. D.; Wang, X. *Powder Technol.* **2007**, *172*, 27.

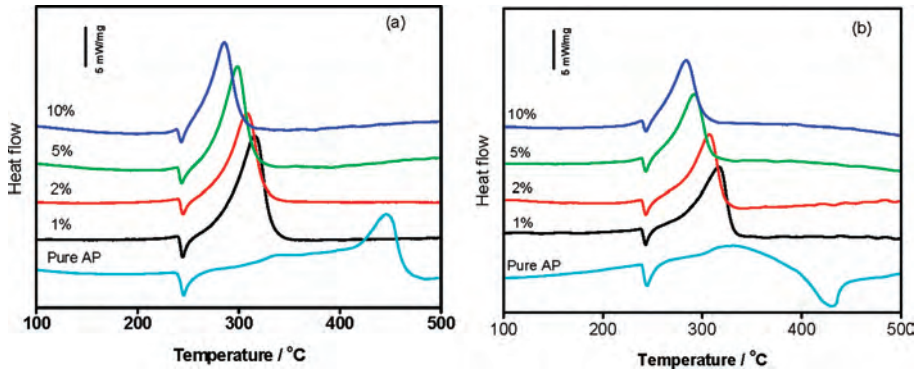

Figure 8. DSC curves for the decomposition of AP with different mass percent of sample I under the measurement conditions (a) with and (b) without lids.

increasing the amounts of CoO in AP, the decomposition heat reduced, which was accompanied by a decrease in the maximum decomposition temperature (Figure 8). Specifically, upon addition of 10 wt % CoO nanocrystals (sample I), the decomposition heat was 1162 J/g with lids, which reduced to 809 J/g without lids, while the maximum AP decomposition temperature decreased to 285 °C.

Intrinsically, the thermal decomposition of AP is closely associated with the chemical nature of the nanocrystal additives,[36] although there still remain some unsolved issues. Duan et al.[35c] studied the impacts of nanosized MgO additives on the AP decomposition and found that the AP decomposition temperature gradually increases with MgO additives, while the decomposition heat decreases. By contrast, when AP is mixed with Y_2O_3 additives, thermal decomposition of AP shows an opposite trend[37] as characterized by a lowered decomposition temperature of AP and an increased decomposition heat. Several assumptions[30] have been proposed to explain the mechanism of the AP decomposition with oxide additives, which include the formation of easily melting eutectics between oxide additives and ammonium perchlorate or intermediate amine compounds, and the release of O^{2-} ions. As analyzed above, AP decomposition involves two crucial steps: (1) ammonia oxidation and (2) dissociation of ClO_4^- species into ClO_3^- and O_2.[38] In the first step, both CoO and Co_3O_4 exhibit high and stable catalytic activity and selectivity toward ammonia oxidation,[24] thus promoting the AP decomposition. In the second step, the ClO_4^- species in the presence of the oxide additives would decompose as follows:[39]

$$ClO_4^- + 2e_{(oxide)} \rightarrow ClO_3^- + O_{(oxide)}^{2-} \rightarrow ClO_3^- + \frac{1}{2}O_2 + 2e'_{(oxide)} \quad (3)$$

where $e_{(oxide)}$ is an electron donated by the oxide additives, $O_{(oxide)}^{2-}$ is an oxygen attracted by the oxide additives, and $e_{(oxide)}'$ denotes the electrons accepted by oxide additives. As stated above, the surfaces of our X-ray "pure" CoO nanocrystals were terminated by an extremely thin Co_3O_4 surface layer. From the left-hand side of eq 3, CoO could donate electrons to initiate the decomposition of ClO_4^-, while Co_3O_4 accepted the produced electrons, pushing the decomposition reaction to proceed toward the right-hand side of eq 3. Consequently, AP decomposition rate is significantly enhanced by the unique composite nanostructure of the present samples. Although the catalytic roles that oxide additives play in the AP decomposition are still not fully understood, the variations of decomposition temperature and heat with the mass percent of CoO nanocrystals seem to be caused by the formation of the intermediate product and the release of O^{2-} ions. It is reasonable that the reduction of decomposition heat is related to the increase of intermediate eutectics, while the decreased decomposition temperature of AP with additive mass might be related to the oxidized ammonium radicals by oxygen as is released from highly reactive Co_3O_4 thin layers on surfaces of CoO nanocrystals or from the decomposition of cobalt perchlorate.[40]

Kinetic parameters for AP decomposition with CoO additives were calculated from the exothermic peak temperature dependence as a function of heating rate. Figure 9 shows the DSC curves of the mixtures of AP with the samples at different heating rates in crucibles with lids. First, at the same heating rate, the peak temperatures of AP decomposition varied slightly from each other for the CoO additives (samples I and II). In the presence of sample I, AP decomposition released a smaller heat than that with sample II. These observations imply that particle size of CoO additives plays a crucial role in the kinetic parameters for AP decomposition, similar to those reported using many other transition metal oxide additives.[35a,b] Second, it is seen from Figure 9 and Supporting Information that the decomposition temperature of AP is dependent on the heating rate with or without CoO additives. The relationship between decomposition temperature and heating rate can be described by Kissinger correlation

$$\ln \frac{\beta}{T_p^2} = \ln \frac{AR}{E_a^2} - \frac{E_a}{RT_p} \quad (4)$$

where β is the heating rate in degrees Celcius per minute, T_p is the peak temperature, R is the ideal gas constant, E_a is

(36) Brill, T. B.; Brush, P. J.; Patil, D. G. *Combust. Flame* **1993**, *94*, 70.
(37) Chen, W. F.; Li, F. S.; Liu, L. L.; Li, Y. X. *J. Rare Earth* **2006**, *24*, 543.
(38) El-Awad, A. M.; Said, A. A.; Abd El-Salaam, K. M. *Thermochim. Acta* **1988**, *126*, 17.
(39) Shimokawabe, M.; Furuichi, R.; Ishii, T. *Thermochim. Acta* **1977**, *20*, 347.
(40) Solymosi, F.; Gera, L. *J. Phys. Chem.* **1971**, *75*, 491.

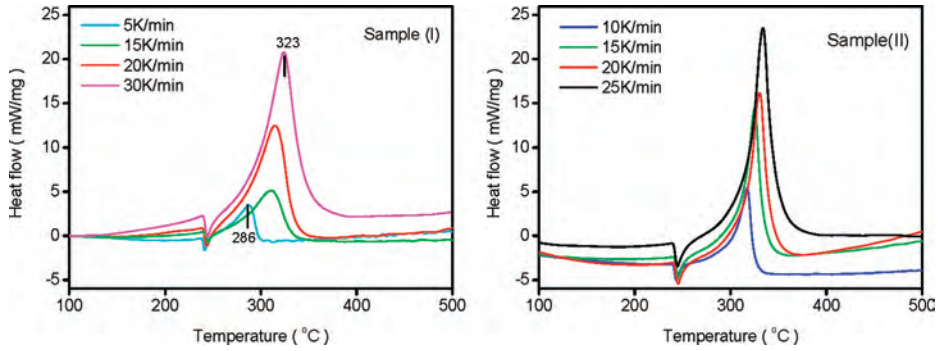

Figure 9. DSC curves of AP with additives of samples I and II at given heating rates in crucibles with lids.

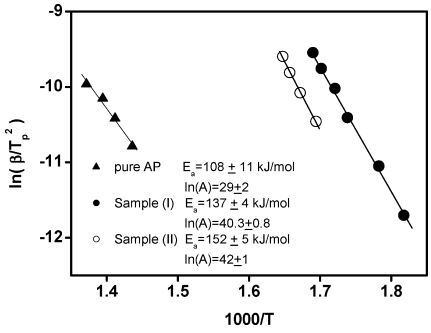

Figure 10. Dependence of ln β/T_p on $1/T_p$ for AP decomposition. Scatter points are experimental data and lines denotes the liner fitting results.

the activation energy, and A is the pre-exponential factor. According to the eq 4, the term ln β/T_p varies linearly with $1/T_p$, yielding the kinetic parameters of activation energy from the slope of the straight line and of pre-exponential factor from the intercept. Figure 10 shows the experimentally measured ln β/T_p versus $1/T_p$ with and without CoO additives. For pure AP, the activation energy of HTD was calculated to be 108 ± 11 kJ/mol, which is close to the value previously reported in literature.[41] In the presence of CoO additives, the activation energy of AP decomposition became as large as E_a = 137 ± 4 kJ/mol with sample I or 152 ± 5 kJ/mol with sample II. The increased activation energy for AP decomposition has been studied by several researchers.[34,42] Ninan et al. concluded that the increased activation energy is caused by the kinetic compensation effect.[43] The activation energy of AP decomposition is not a parameter that describes the decomposition process by itself. The value of pre-exponential factor A should also be considered. For the reaction system in which compensation effect affects the decomposition behavior significantly, the ratio of $E_a/\ln(A)$ could be used to describe the reactivity.[44] Usually, a larger ratio means greater stability of the reactant. For our samples, the ratios of $E_a/\ln(A)$ are 3.7, 3.6, and 3.4 for pure AP, AP with sample II, and AP with sample I, respectively. Obviously, sample I shows a better catalytic activity toward AP decomposition than that shown by sample II.

4. Conclusions

CoO nanocrystals were prepared by a solvothermal reaction. The average particle sizes of CoO nanocrystals were about 22 nm prepared in pure ethanol solution or 44 nm in the presence of a small amount of hydrazine. Several combined characterization techniques demonstrate that all as-prepared samples were CoO nanocrystals which were terminated by thin layers of Co_3O_4. The as-prepared samples were explored as the additives to promote the AP decomposition. It is found that the decomposition heat of AP was significantly improved as followed by an apparent decrease in the maximum decomposition temperature in comparison with those of the additives of 18 nm Co_3O_4 of pure phase. The decomposition temperature and heat of AP systematically varied with the content of CoO additives and the use of lids, which are ascribed to the dual effects of intermediate product and the release of O^{2-} ions from the surface Co_3O_4 thin layers.

Acknowledgment. This work was financially supported by NSFC under the contract (Nos. 20671092, 20771101, 20773132), National Basic Research Program of China (2009CB939801), Science and Technology Program from Fujian Province (Nos. 2006J0178, 2006L2005), FJIRSM (No. SZD-08002-3), and Directional program of CAS (No. KJCXZ-YW-MO5).

Supporting Information Available: IR spectrum of the precursor when using Method II, DSC curves of pure AP at different heat rates, and comparison of DSC curves of AP with CoO and Co_3O_4 nanocrystalline additives. This material is available free of charge via the Internet at http://pubs.acs.org.

IC8008283

(41) (a) Oxley, J. C.; Smith, J. L.; Valenzuela, B. R. *J. Energy Mater.* **1995**, *13*, 57. (b) Morisaki, S.; Komamiya, K. *Thermochim. Acta* **1975**, *12*, 239.

(42) (a) patil, P. R.; Krisnamurthy, V. N.; Joshi, S. S. *Propellants, Explos., Pyrotech.* **2006**, *31*, 42. (b) Solymosi, F.; Bansagi, T. *Kinet. Catal.* **1963**, *4*, 73.

(43) Ninan, K. N. *Indian J.Chem., Sect. A: Inorg., Bio-inorg., Phys., Theor. Anal. Chem.* **1998**, *37*, 295.

(44) Andricic, B.; Kovacic, T.; Klaric, I. *Polym. Degrad. Stab.* **2003**, *79*, 265.